Journal of Materials Science & Technology 156 (2023) 20–31

Contents lists available at ScienceDirect

Journal of Materials Science & Technology

journal homepage: www.elsevier.com/locate/jmst

Research Article

Anti-inflammatory and anabolic biphasic scaffold facilitates osteochondral tissue regeneration in osteoarthritic joints

Xiangbo Meng[a,d], Ling Li[a,d], Cuishan Huang[a,d], Keda Shi[a,d], Qingqiang Zeng[a], Chunyi Wen[e], Sibylle Grad[b], Mauro Alini[b], Ling Qin[a,c,d,*], Xinluan Wang[a,c,d,*]

[a] Translational Medicine R&D Center, Institute of Biomedical and Health Engineering, Shenzhen Institutes of Advanced Technology, Chinese Academy of Sciences, Shenzhen 518055, China
[b] AO Research Institute Davos, Clavadelerstrasse 8, Davos Platz 7270, Switzerland
[c] Musculoskeletal Research Laboratory, Department of Orthopaedics & Traumatology, The Chinese University of Hong Kong, Hong Kong SAR 999077, China
[d] CAS-HK Joint Lab of Biomaterials, Joint Laboratory of Chinese Academic of Science and Hong Kong for Biomaterials, Translational Medicine Research and Development Center, Shenzhen Institutes of Advanced Technology of Chinese Academy of Sciences and The Chinese University of Hong Kong, China
[e] Department of Biomedical Engineering, Faculty of Engineering, The Hong Kong Polytechnic University, Hong Kong SAR 999077, China

ARTICLE INFO

Article history:
Received 15 May 2022
Revised 19 January 2023
Accepted 19 January 2023
Available online 22 March 2023

Keywords:
Biphasic scaffold
Osteochondral defect
Osteoarthritis
Kartogenin
Cinnamaldehyde
Anti-inflammation

ABSTRACT

Osteochondral defects (OCD) are common but difficult to heal due to the low intrinsic repair capacity of cartilage and its complex hierarchical structure. In osteoarthritis (OA), OCD become more challenging to repair as both cartilage and subchondral bone regeneration are further impaired due to the arthritic environment. Numerous biomaterials have been developed and tested in osteochondral defects while ignoring the inflammatory environment. To target this challenging underlying pathophysiology, we designed and fabricated a biphasic porous and degradable scaffold incorporating anti-inflammatory and anabolic molecules by low-temperature rapid prototyping technology, and its effects on promoting osteochondral regeneration were evaluated using our well-established OA-OCD rabbit model. The biphasic porous scaffolds consisted of poly lactic-co-glycolic acid (PLGA) with kartogenin (KGN) for cartilage repair and PLGA and β-calcium phosphate (PLGA/β-TCP) with cinnamaldehyde (CIN) for subchondral bone repair. KGN is a molecule for promoting chondrogenesis and CIN is a phytomolecule for enhancing osteogenesis and alleviating inflammation. The biphasic scaffolds PLGA/KGN-PLGA/β-TCP/CIN (PK/PTC) with bio-mimic structure provided stable mechanical properties and exhibited excellent biocompatibility to support cell adhesion, proliferation, migration, and distribution. Furthermore, KGN and CIN within biphasic scaffolds could be released in a controlled and sustained mode, and the biphasic scaffold degraded slowly *in vitro*. Evaluating the repair of 16-weeks post-implantation into critically sized OA-OCD rabbit models revealed that the biphasic scaffold could promote subchondral bone and cartilage regeneration, as well as reverse subchondral osteosclerosis caused by inflammation *in vivo*. These findings support the utilization of the PK/PTC scaffold for osteochondral regeneration and provide a promising potential strategy for clinical application for the treatment of patients with OA-OCD.

1. Introduction

Osteoarthritis (OA) also known as a degenerative joint disease, involves the gradual and progressive wearing of the cartilage and concomitant subchondral bone remodeling, which often results in osteochondral defect (OCD) [1,2]. An OCD refers to a focal area of damage that involves both the cartilage and its underlying subchondral bone. OCD can also occur from an acute traumatic injury to the knee or an underlying disorder of the bone [3]. Due to its avascular tissue, low cell density, and low metabolic activity, cartilage cannot regenerate after degeneration. Therefore, the treatment of OCD in OA (OA-OCD) remains a significant clinical challenge [4]. The current clinical strategies used to treat cartilage defect, include marrow stimulation technology (MST) for lesion sizes smaller than 2 cm^2, autograft transplantation, autologous chondrocyte implantation (ACI) or osteochondral allograft (OCA) for lesion size larger than 2 cm^2 [5]. Although successful in some aspects, each of these technologies has its limitations. For example, MST results in fibrocartilage and not in hyaline cartilage tissue [6]; au-

* Corresponding authors at: Translational Medicine R&D Center, Institute of Biomedical and Health Engineering, Shenzhen Institutes of Advanced Technology, Chinese Academy of Sciences, Shenzhen 518055, China.
E-mail addresses: lingqin@cuhk.edu.hk (L. Qin), xl.wang@siat.ac.cn (X. Wang).

https://doi.org/10.1016/j.jmst.2023.01.035
1005-0302/

tologous graft transplantation induces donor site morbidity, incomplete fusion with the host bone, and high transplantation failure rate [7]; regarding ACI, the deficiency of therapeutic chondrocytes seriously affects the effectiveness and quality of repair [8].

Tissue engineering approaches have been developed as potential solutions for OCD regeneration [9,10]. To date, efforts have mainly focused on the development of osteochondral graft substitutes [11,12]. Biomaterial scaffolds are designed and manufactured to provide a physiological environment to support cell activities and control the release of bioactive ingredients for tissue regeneration [13,14]. The bioactive ingredients can be incorporated into the scaffolds, and then implanted into the OCD to promote osteochondral regeneration [15,16]. Poly(lactic-co-glycolic acid) (PLGA) and β-Tricalcium phosphate (β-TCP) are well known for their excellent biocompatibility, biosafety, and biodegradability [17,18]. Our previous studies showed that the porous PLGA/TCP (PT) scaffold exhibited good biocompatibility, osteoconductivity, and biodegradability both *in vitro* and *in vivo* [19]. Kartogenin (KGN), a small heterocyclic compound, can stimulate chondrogenic differentiation *in vitro* and induce cartilage formation *in vivo* [20,21]. Cinnamaldehyde (CIN) is a phoytomolecule from traditional Chinese herbal medicine, known to regulate angiogenesis and promote osteogenic mineralization *in vitro* [22,23]. In our previous study, we found that CIN could inhibit the inflammation of human synovial cells by regulating the Jak/Stat pathway [24]. Based on these pieces of research, we hypothesized that KGN and CIN could be incorporated into a biomaterial scaffold with bioactivity preservation and controlled release to promote osteochondral regeneration in an inflammatory environment.

In this study, a biphasic scaffold incorporating KGN and CIN was designed and fabricated via low-temperature 3D printing technology to preserve the bioactivity of KGN and CIN for facilitating the repair of osteochondroal defect using our previously established OA-OCD rabbit model [25].

2. Materials and methods

2.1. Preparation of biphasic scaffolds

Composite porous scaffolds were prepared in a low-temperature 3D printing machine (SUNP Alpha-BP21, SUNP BIOTECH, Beijing, China). The process starts with a 3D structure model design using SUNP Biomaker software, followed by applying slicing to prepare 2D layer-by-layer slices for 3D printing. The printing parameters were set up at a print speed of 20 mm s^{-1}, extrusion speed of 0.8 mm^3 s^{-1} and line distance of 1.0 mm, layer height of 0.12 mm. The PLGA (lactide/glycolide ratio of 75:25, average molecular weight (Mw) = 15 w Dalton, viscosity=1.18 dL g^{-1}) (Shandong academy of pharmaceutical sciences, Jinan, China) was dissolved in 1, 4-dioxane (Shanghai Ling Feng Chemical Reagent Co., Ltd, Shanghai, China) and formed a 10% (w/v) homogeneous solution. Then, β-tricalcium phosphate (β-TCP, Aladdin) was mixed into the homogeneous solution at a ratio of 4:1 (w/w). The mixture was stirred overnight to form a uniform liquid paste (PT paste) using a magnetic stirrer. CIN (Chengdu Ruifen Si Biological Technology Co., Ltd., Chengdu, China) was dissolved in 1,4-dioxane at the concentration of 40 mg mL^{-1} and CIN solution was added to the PT paste (PTC) to finally yield 0.5% drug concentration. The same method was used to prepare the PLGA paste with 1.0% KGN (MedChem Express, USA) (PK paste). Firstly, the PTC paste was spurted layer-by-layer in a computer-driven nozzle with a diameter of 600 μm to form the PTC scaffold (volume 20 mm × 20 mm × 10 mm) at −30 °C, and then the PK paste was spurted in the same conditions to form biphasic scaffolds (volume 20 mm × 20 mm × 20 mm) loaded with KGN and CIN, named PK/PTC scaffold. Finally, the PK/PTC scaffolds were lyophilized in a freeze dryer for 48 h (Bo Yi Kang FD-1-50, China) under a vacuum of 50 Pa pressure. According to the above method, the scaffold without KGN and CIN was prepared and named a PTP scaffold.

2.2. Characterization of the porous biphasic scaffolds

2.2.1. Morphological characterization

The microstructure of the biphasic scaffold was observed under scanning electron microscopy (SEM, ZEISS Supra 55). Three samples (5 mm × 5 mm × 1 mm) were sliced and mounted directly on the sample holder. Before performing SEM, the surface of the scaffold was coated with a thin layer of gold to provide electrical conductivity. Then, the scaffolds were placed in an SEM chamber and images were acquired using an In-lens SE detector (EHT: 5 kV, WD: 4.2 mm). The average pore size of the scaffold was determined from the SEM photographs using an Image-Pro-Plus 6.0. In addition, the porous biphasic scaffolds were scanned using a micro-CT (skyscan 1176, Bruker, Germany) with a source voltage of 40 kV, source current of 600 μA, and voxel size of 9 μm. After scanning, a three-dimensional (3D) image of the porous biphasic scaffold was reconstructed.

2.2.2. Porosity

The porosity of the biphasic scaffold was determined by liquid displacement methods [26]. The scaffolds were cut into cubes (5 mm × 5 mm × 5 mm, n = 3), and the volume and weight were recorded as V_s and W_1. Next, the scaffold was immersed in ethanol. Then the scaffold had been taken out until there was no bubbling, and the weight was recorded as W_2 [27]. The porosity was calculated as follows:

$$\text{Porosity } (\%) = \frac{(W_2 - W_1)/\rho_e}{V_s} \times 100$$

W_1: the scaffold weight; W_2: the ethanol-saturated scaffold weight; ρ_e: the density of ethanol; V_s: the volume of the scaffold

2.2.3. Mechanical properties

The scaffolds (n = 3) were cut into 5 mm × 5 mm × 5 mm cubes. The mechanical properties were assessed using a mechanical testing machine (Instron E300, USA) with a 2800 N load cell. At the start of the test, the scaffold was in an undeformed state (zero displacement) and the loading point contacted the scaffold with a small preload (0.1 N) to keep the scaffold in place. Then confined compression was performed at a displacement rate of 1 mm min^{-1}, until the thickness of the sample becomes 70% of the initial thickness, and the force value was recorded in the compression process to obtain the load-displacement curves. The load-displacement curves were transformed into scaffold stress–strain curves according to the International Organization for Standardization (ISO 844:2004). Young's modulus was calculated from the linear region of the stress–strain curve. The yield point was found using Vernier Graphical Analysis (Vernier Science Education, USA), and the compressive strength at the yield point was used to compare the difference among different groups.

2.2.4. Scaffold degradation and drug release

The scaffolds were cut into cubes (5 mm × 5 mm × 5 mm) and put into glass bottles (n = 3), and then the scaffold was infiltrated with a phosphate-buffered saline (PBS) solution (pH = 7.0), according to mass volume ratio of 1:15 (w/v). The scaffolds were shaken in a thermostatic water bath bed at 37°C and refreshed with PBS every week. The degradation solution was collected to test the pH value via a pH meter and analyze the released drug concentration via high-performance liquid chromatography (HPLC).

2.3. In vitro *cellular evaluation of porous biphasic scaffolds*

Rat bone marrow mesenchymal stromal cells (rBMSCs) were used to assess the biocompatibility of the porous biphasic scaffolds. Briefly, the cells were cultured in Dulbecco's Modified Eagle Medium (DMEM), supplemented with 10% (v/v) fetal bovine serum, 1 mM glutamine, and 1% (v/v) penicillin/streptomycin (all from Cyagen Biosciences, USA) in a humidified 5% CO_2 incubator at 37 °C. The porous biphasic scaffolds (ø 6 mm × *H* 1 mm, $n = 3$) were immersed in 70% alcohol overnight and sterilized by UV irradiation 3 times 30 min. The rBMSCs were seeded on top of the scaffolds at a density of 1×10^4 cells scaffold^{-1} in a 96-well plate. After 72 h, the medium was discarded, the scaffold washed 3 times with PBS, and then fixed with 4% paraformaldehyde for 15 min and were washed 3 times with PBS. The scaffolds were finally stained using DAPI solution at room temperature for 15 min in the dark and washed twice with PBS. The cell adhesion on the porous biphasic scaffolds was observed with SEM (ZEISS Supra 55) and fluorescence microscopy (Leica Dmi8, Germany).

2.4. *Evaluation of intervention effects of porous biphasic scaffolds* in vivo

2.4.1. *Animal models and experimental design*

A total of 24 male New Zealand white rabbits (body weight: 2.0–2.5 kg, age: 6 months) were purchased from Southern Medical University Laboratory Animal Center (Guangzhou, China) and maintained in the normal breeding room at Shenzhen-Peking University-Hong Kong University of Science & Technology (Shenzhen-PKU-HKUST) Medical Center. In this study, all the procedures for animal experiments were approved by the institutional animal care and use committee of the Shenzhen Institutes of Advanced Technology, Chinese Academy of Sciences (SIAT-IRB-170718-WXL-A0360). The rabbits were randomly divided into three groups: (1) empty defect as the control group ($n = 8$); (2) PTP scaffold implantation as the PTP group ($n = 8$); (3) PK/PTC scaffold implantation as PK/PTC group ($n = 8$). The PK/PTC scaffold and PTP scaffold were trimmed into a cylinder with 3.2 mm diameter and 3 mm height, where the height of the PK layer or PLGA layer was 1 mm and the height of the PTC layer or PT layer was 2 mm.

2.4.2. *Surgical procedure and scaffold implantation*

The OA-OCD model was established to assess the repair effect of the porous biphasic scaffolds *in vivo*. First, OA was induced by intra-articular injection of papain enzyme (12.5 mg mL^{-1}) in the right knee joints at the dose of 0.2 mL on the 10th and 7th days before implantation [28,29]. As a control, the same dose of 0.9% saline was injected into the left knee joints at the same time. Then, the OCD model was made according to the following protocol. The animals were anesthetized by an injection of 3.0% (w/v) pentobarbital sodium (50 mg kg^{-1}) into the ear vein. After carefully cleaning the surgery site, the knee joint of the rabbit was cut open to expose the femur trochlear groove. The OCD (3.2 mm in diameter and 3 mm in depth) was created on the femur trochlear groove of the rabbits by a drill. During the drilling process, the defects were irrigated with saline solution to prevent local overheating. Then the sterilized scaffolds were press-fit into pre-drilled cavities in the defect sites. Subsequently, the incisions were sutured layer by layer using a degradable suture (4-0 silk suture, Jinhuan, Shanghai, China). After the operation, penicillin (50000 IU kg^{-1}) and gentamicin (5 mg kg^{-1}) was intramuscularly injected for 3 days to prevent bacterial infections. At 16 weeks post-surgery, the joint samples were harvested. After surgery, the body weight and knee width of rabbits were measured once a week for 16 weeks. Three days and ten days prior to sacrifice, the rabbits received subcutaneous injections of calcein (5 mg kg^{-1}, Sigma Aldrich) and xylenol orange (90 mg kg^{-1}, Sigma Aldrich) to allow for histological measures of bone formation.

2.4.3. *Micro-computed tomography (micro-CT) analysis*

The joint samples were fixed in 4% (w/v) paraformaldehyde for 3 days, then stored in 70% ethanol solution at 4 °C. The samples ($n = 8$ for each group) were scanned using a micro-CT (SkyScan 1176, Bruker, Kontich, Belgium) with a voltage of 65 kV, a current of 385 μA, an integration time of 300 ms, an aluminum filter of 1 mm, and a pixel size of 18 μm. All scan data were acquired and reconstructed using Skyscan software. The threshold was adjusted at 75–255 HU to differentiate mature bone from soft tissue according to our previous work [30,31]. The newly formed bone in the defect region was obtained to quantify bone mineral density (BMD) and bone volume/tissue volume (BV/TV).

2.4.4. *Histological evaluation*

After the micro-CT analysis, four samples from each group were decalcified in 10% (w/v) ethylene diamine tetraacetic acid (EDTA), dehydrated by a series of ethanol, embedded in paraffin, and cut into pieces longitudinally with an approximate thickness of 5 μm using a paraffin microtome (Leica RM 2235, Germany). Sections were stained with safranin o-fast green (S-F), toluidine blue (T-B), and hematoxylin and eosin (H-E) to assess the new tissue in the defect site. The histological sections were blindly scored by three evaluators using a modified O'Driscoll histologic scoring [25], and scores were averaged. The optical density of sulfated glycosaminoglycan (sGAG) was semi-quantitatively calculated using Image-pro plus 6.0 [22,26].

2.4.5. *Dynamic histomorphometry*

After the micro-CT analysis, four samples from each group were embedded in MMA and cut at 8 μm thickness using a tungsten steel knife (Leica 26166, Germany). Undecalcified sections were observed by fluorescence microscopy (Leica Dmi8, Germany) to determine the mineral apposition rate (MAR), and bone formation rate (BFR/BS) of new bone formation by monitoring the distance and perimeter between the two labels. The 5 μm-thick sections were cut from the MMA-embedded samples and stained with Goldner's trichrome to allow for measurement of osteoid surface (OS/BS) in the newly regenerated tissues.

2.4.6. *Immunohistochemistry*

For immunohistochemical (IHC) staining of type I collagen (COL I), type II collagen (COL II), and matrix metalloproteinase-3 (MMP-3), the decalcified 5 μm sections ($n = 4$) were dewaxed in decreasing concentrations of alcohol and rehydrated. The sections were immersed in 3% hydrogen peroxide for 10 min (protected from light) and blocked in 5% (v/v) goat serum solution for 15 min. After enzymatic antigen retrieval, the sections were incubated with primary antibodies against COL I (NB600-450, Novus), COL II (NBP600-844, Novus), and MMP-3 (66338-1-lg, Proteintech) for 12 h in a 4 °C refrigerator. After washing with PBS, they were incubated with horseradish peroxidase-conjugated immunoglobulin G (IgG) and then incubated with 3, 3-diaminobenzidine tetrahydrochloride (DAB) for visualization. Nuclei were counterstained with hematoxylin.

2.5. *Statistics*

Data were presented as mean ± SD. Statistical analysis was performed using GraphPad Prism 6.0 (GraphPad Software Inc., San Diego, CA, USA). Two-way ANOVA followed by *post hoc* Fisher's LSD test was used to evaluate differences between experimental groups and the differences were considered significant when $p < 0.05$.

Table 1
Macropore size, porosity, compressive strength, and Young's modulus of biphasic scaffolds.

	Macropore size (μm)	Porosity (%)	Compressive strength (MPa)	Young's modulus (MPa)
PLGA	563 ± 47	74.93 ± 3.61	0.85 ± 0.08	18.22 ± 2.62
PLGA/KGN	532 ± 28	70.15 ± 4.36	0.80 ± 0.07	17.58 ± 2.12
PLGA/TCP	485 ± 20	68.91 ± 4.02	1.39 ± 0.15	28.08 ± 3.73
PLGA/TCP/CIN	473 ± 13.19	67.59 ± 2.32	1.27 ± 0.12	28.14 ± 2.86

Data are expressed as means ± SD ($n = 3$).

3. Results

3.1. Characterization of the porous biphasic scaffolds

Porous biphasic scaffolds are advantageous for osteochondral tissue engineering applications, as they can mimic the native structure for each tissue type [32]. As shown in Fig. 1(A), the SEM images showed that the PLGA layer exhibited a porous structure with a smooth surface. The pores inside the PLGA layer were interconnected with a porosity of 74.93% ± 3.61% and a macropore size of 563 ± 47 μm (Table 1). The PLAG/β-TCP (PT) layer had a rough surface owing to the β-TCP particles and a fully interconnected porous pattern. The pores of the biphasic scaffold were divided into macropores (pores > 100 μm in size) and micropores (pores < 50 μm in size) [33]. The macropore size of this phase was 485 ± 20 μm and its porosity was 68.91% ± 4.02%. Numerous micropores were observed on the wall surface of the scaffold framework, which resulted in a larger surface area, and the pore sizes of the micropores were ranging from 5 to 20 μm. A good integration between the PLAG layer and the PT layer could be found in the SEM image and micro-CT image (Fig. 1(B)), which is considered to be an ideal structure for osteochondral tissue engineering. As shown in Fig. 1(C–E), the compressive strength and Young's modulus of the PLGA/KGN (PK) layer were 0.80 ± 0.07 and 17.58 ± 2.12 MPa, with no significant difference as compared with the PLGA layer. The compressive strength and Young's modulus of the PLAG/β-TCP/CIN (PTC) layer were 1.27 ± 0.12 and 28.14 ± 2.86 MPa, respectively, which was also not different from the PT layer (Table 1). The incorporated bioactive molecules (KGN or CIN) did not alter the structural and mechanical properties or the porosity of the PLGA layer or PT layer.

The biodegradation of the porous biphasic scaffold is one of the key factors which can provide a desirable micro-environment that allows neo-tissue to be generated properly for repairing and replacing damaged tissues [34]. As shown in Fig. S1 in the Supporting Information, the scaffold underwent slow degradation *in vitro*. The pH values of the degradation medium were measured up to 236 days. The pH value of the degraded medium maintained above 7.0 for 37 days, then declined and reached the lowest value (pH = 2.28 at day 159 for PK, pH = 2.28 at day 194 for PLGA, pH = 3.27 at day 201 for PT, pH = 3.40 at day 201 for PTC), and finally raised to about 6.41 at day 236 (Fig. 1(F)).

With the degradation of the biphasic scaffold, the bioactive molecule (KGN and CIN) in the scaffold was released, whereby the cumulative release rate of KGN was 84.59%, and the cumulative release rate of CIN was 85.92 % (Fig. 1(G)).

The bone marrow mesenchymal cells from rats (rBMSCs) were used to evaluate the cell adhesion on biphasic scaffolds (Fig. 1(H)). It was found that the biphasic scaffolds were favorable for cell adhesion with cells attached to the surface of the scaffolds.

3.2. Macroscopic observation

The rabbit model was used to assess the OA-OCD regeneration for biphasic scaffolds (Fig. 2(A)). No migration of the scaffold was observed at the end of this study. Sixteen weeks after implantation, the weight and knee width of rabbits showed that the animals in different groups had good vital signs, without significant differences among groups (Fig. 2(B)). Compared to the non-OA microenvironment, the cartilage surface in the OA environment was eroded by papain (Fig. 2(C)). Macroscopic observation showed that the defects of the PK/PTC scaffold group were filled with newly formed tissue in both OA and non-OA micro-environments. Specifically, the formation of cartilage-like tissue similar to the adjacent native cartilage was observed in the PK/PTC scaffolds, and the ICRS scores of the OA and the non-OA micro-environments were 7.38 ± 0.99 and 7.28 ± 1.39, respectively. However, the new-formed tissue was less transparent in the PTP group and control group, an indication of incomplete repair, and the ICRS scores of the PTP group and the control group in the OA environment were 6.50 ± 1.32 and 6.0 ± 0.86, and their ICRS scores in the non-OA environment were 7.57 ± 0.72 and 7.71 ± 2.31, respectively (Fig. 2(D)).

3.3. Micro-CT analysis: enhanced subchondral bone repair in PK/PTC scaffolds

The newly formed tissue was evaluated by micro-CT. As shown in Fig. 3(A), the defect in the PK/PTC group was filled with new bone 16 weeks after implantation. For the control group, the self-repair of subchondral bone was limited and there was a large cavity in the defect region. For the PTP group, the defect region was incomplete, with the new bone mainly distributed around the bottom and the side of the defects. As shown in Fig. 3(B–D), in the control group, the BV/TV of the new bone in the OA environment was 28.3% lower than that in the non-OA environment, and the BMD of the new bone in the OA environment was 26.7% higher than that in the non-OA environment. This suggests that new bone formation was decreased and BMD of subchondral bone was increased in the inflammatory environment. Regardless of the OA environment or non-OA environment, the BV/TV of the PK/PTC group was higher than that of the PTP group and the control group. In addition, in the PK/PTC group, the BMD of the new bone in the OA microenvironment was close to that of the non-OA group, and the BMD of the new bone was similar to that of the host bone.

3.4. Histological analysis: PK/PTC scaffolds promoted OCD regeneration

The histological staining analysis confirmed that the PK/PTC scaffolds were able to improve the regeneration of cartilage in the OA and non-OA micro-environments, compared with the PTP group and control group (Fig. 4(A)). At 16 weeks post-implantation, new cartilage was observed in the OCD site of the PK/PTC group, and the new cartilage showed strong staining of safranin o-fast green (S-F), toluidine blue (T-B), and hematoxylin and eosin (H-E). At high magnification, the arrangement of chondrocytes in the new cartilage shows a pattern similar to hyaline cartilage. The quantitative scoring of histological staining was performed according to the modified O'Driscoll histology score (O'Driscoll score). The PK/PTC scaffold showed significantly (19.44%) higher scores than the control group in the OA micro-environment (Fig. 4(B)). In addition, S-

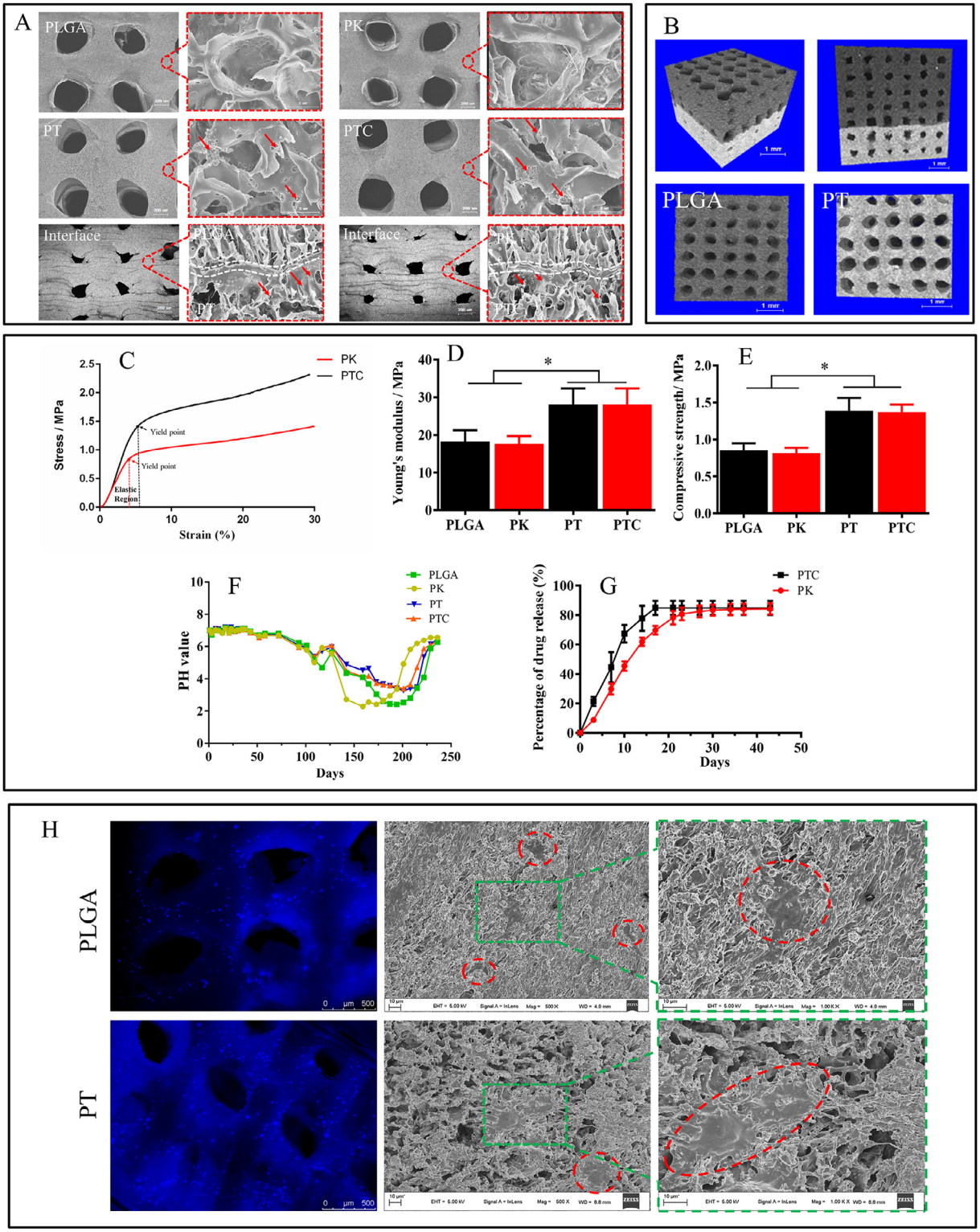

Fig. 1. Morphology, degradation, drug release, and cytocompatibility *in vitro* evaluation of the porous biphasic scaffold. (A) SEM image at high magnification showed a large number of micropores, red arrow: β-TCP; (B) Micro-CT showed the layered structure of porous biphasic scaffold; (C) The stress–strain curves of PK scaffold and PTC scaffold; (D, E) The Young's modulus and compressive strength of the PLGA/KGN (PK) scaffold or PLGA/TCP/CIN (PTC) scaffold had no difference from those of the PLGA or PLGA/TCP (PT) scaffold; β-TCP can significantly improve the compressive strength and Young's modulus of P scaffold (F, G) The scaffolds degradation and bioactive molecules release curves *in vitro*. (H) DAPI staining and SEM image showed that porous biphasic scaffold was favorable for cell adhesion. Data are shown as mean ± standard deviation, $n = 3$, $^{*}p < 0.05$.

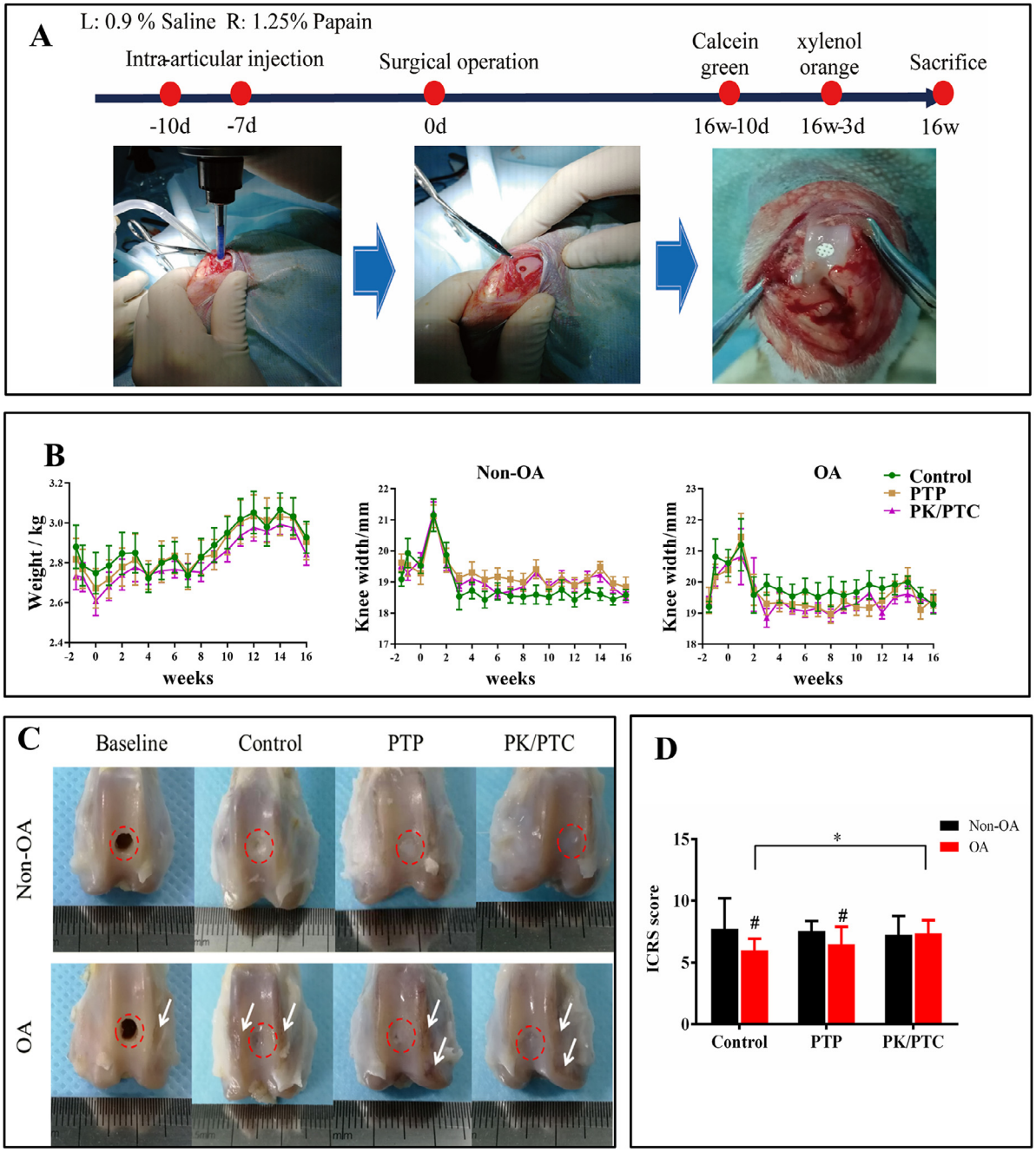

Fig. 2. *In vivo* evaluation of the porous biphasic scaffold. (A) Surgical procedure for OA-OCD model in rabbits; (B) The changes of weight and knee width in rabbits assessed at different time points; (C) Macroscopic observation of the repaired OCD. White arrow: cartilage was damaged by papain; (D) International cartilage repair society (ICRS) macroscopic evaluation of cartilage repair. Data are shown as mean ± standard deviation, $n = 8$, $^{\#}p < 0.05$ vs non-OA; $^{*}p < 0.05$ and $^{**}p < 0.01$.

F staining showed that sGAG in the PK/PTC group was enhanced compared with those in the PTP group and the control group. As shown in Fig. 4(C), the sGAG optical density of neo-cartilage of the PK/PTC scaffold group in the OA environment (51.34 ± 16.87) was 45.5% lower than that in the non-OA environment (94.20 ± 10.09) ($p < 0.05$). In addition, the PK/PTC scaffold also promoted subchondral bone regeneration in the OA microenvironment. There was more newly formed bone in the OCD. Although the PTP scaffold can also support the migration and differentiation of cells and promote subchondral bone regeneration, there is a huge subchondral bone cyst in the subchondral bone, and the edge of the cyst is wrapped by fibrous tissue. In the control group, there were empty cavities and sparse newly formed tissue.

3.5. Dynamic bone histomorphometry analysis: PK/PTC scaffolds enhanced bone remodeling

Bone histomorphology was used to assess the efficiency of bone remodeling [35]. As shown in Fig. 5(A), osteoid and mineralized bone tissues were distinguished via goldner staining. Furthermore, we evaluated the osteoid surface in regenerated bones after 16 weeks of implantation. Compared with the non-OA environment, the osteoid tissue of the control group was reduced by 66.95% in the OA environment (Fig. 5(C)). In the OA environment, the osteoid tissue of the PK/PTC group (21.57 ± 6.08) was 64% higher than that of the PTP group (13.18 ± 2.34). As shown in Fig. 5(B), the new bone was labeled with calcein (green) and xylenol orange dis-

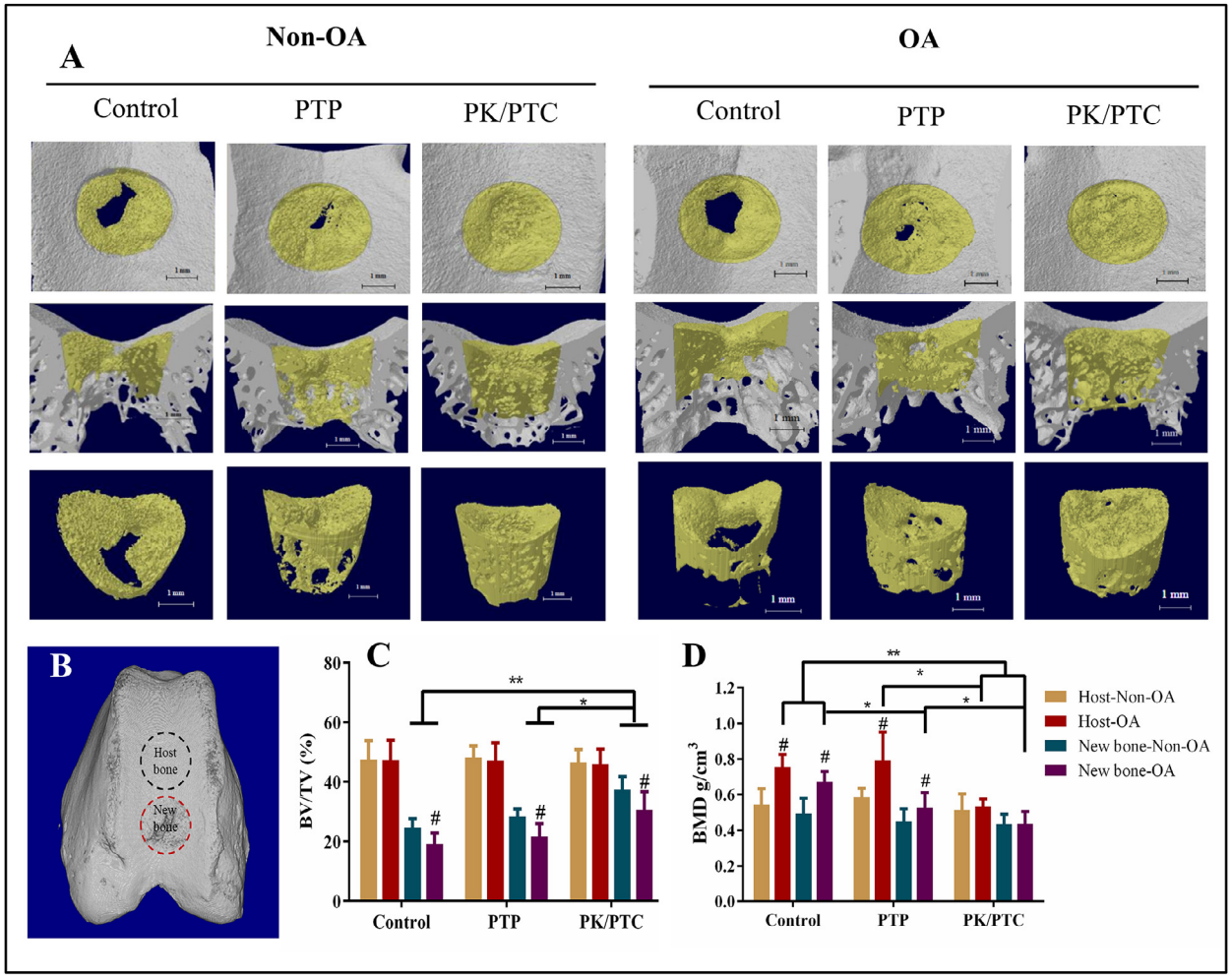

Fig. 3. Micro-CT analysis showed improved subchondral bone repair in PK/PTC scaffolds. (A) The reconstructed images showed the joint surfaces (the first row), transverse surface (the second row), and the regenerated bone (the third row) in the defect area at 16 weeks post-surgery. (B) The reconstructed images showed the joint surfaces, the newly formed bone in the OCD region (new bone), and the host bone. (C) Micro-CT quantitative data showed that the PK/PTC group had a higher bone volume per volume (BV/TV) than the control group and the PTP group. (D) The bone mineral density (BMD) of the PK/PTC group was lower than other groups. Data are shown as mean ± standard deviation, n=8, $^{\#}p < 0.05$ vs non-OA; $^{*}p < 0.05$ and $^{**}p < 0.01$.

odium salt (red). As shown in Fig. 5(D–F), the quantitative results showed that the percent labeled perimeter (L.Pm), mineral apposition rate (MAR), and bone formation rate/bone surface (BFR/BS) of the control group in the OA environment were reduced by 22.22%, 13.60%, and 32.97%, respectively, compared with the non-OA environment. Regardless of the OA environment or non-OA environment, the L.Pm, MAR, and BFR/BS of the PK/PTC group were higher than those of the PTP group and the control group. In the PK/PTC group, the MAR and BFR/BS in the OA microenvironment were higher than those in the non-OA microenvironment.

3.6. IHC staining analysis: PK/PTC scaffolds promoted the secretion of COL I and COL II in the regenerated osteochondral tissue

IHC staining of cartilage and bone-specific proteins was performed to evaluate OCD regeneration. As shown in Fig. 6, compared with the non-OA environment, the COL I and COL II of the new tissues in the control group were reduced by 25.39 % and 23.80% in the OA environment, while MMP3 of the control group increased by 70.03%. In the OA environment, the COL II of the new cartilage in the PK/PTC group (44.63 ± 12.76) was 55.08 % higher than that of the PTP group (20.05 ± 7.91), while the MMP3 of the new cartilage in the PK/PTC group (0.71 ± 0.16) was 76.13% lower than in the PTP group (2.97 ± 0.41).

4. Discussion

The repair of osteochondral defect in osteoarthritis (OA-OCD) remains a major challenge in orthopedics, due to the complex hierarchical structure and low intrinsic repair capacity in cartilage. Here, to target the unique pathology of OA-OCD we successfully fabricated a biphasic porous scaffold incorporating KGN and CIN via low-temperature 3D printing technology to promote OCD regeneration in an inflammatory environment. The pore size, interconnectivity, porosity, and mechanical properties of the biphasic scaffold were suitable for tissue regeneration. The bioactive molecules (KGN and CIN) can be sustained and stably released from the biphasic scaffold. In addition, the PK/PTC scaffold can induce osteochondral regeneration in the rabbit osteoarthritic joints, and reverse subchondral osteosclerosis in an inflammatory environment.

4.1. The biphasic scaffolds promote tissue regeneration

PLGA and TCP were the essential and approved biomaterials used as the local delivery system for incorporating bioactive factors for their controlled release. Their composite scaffold provided the required mechanical strength, and their pore size and degradation rates also favored new bone ingrowth [17,36,37]. Porosity and

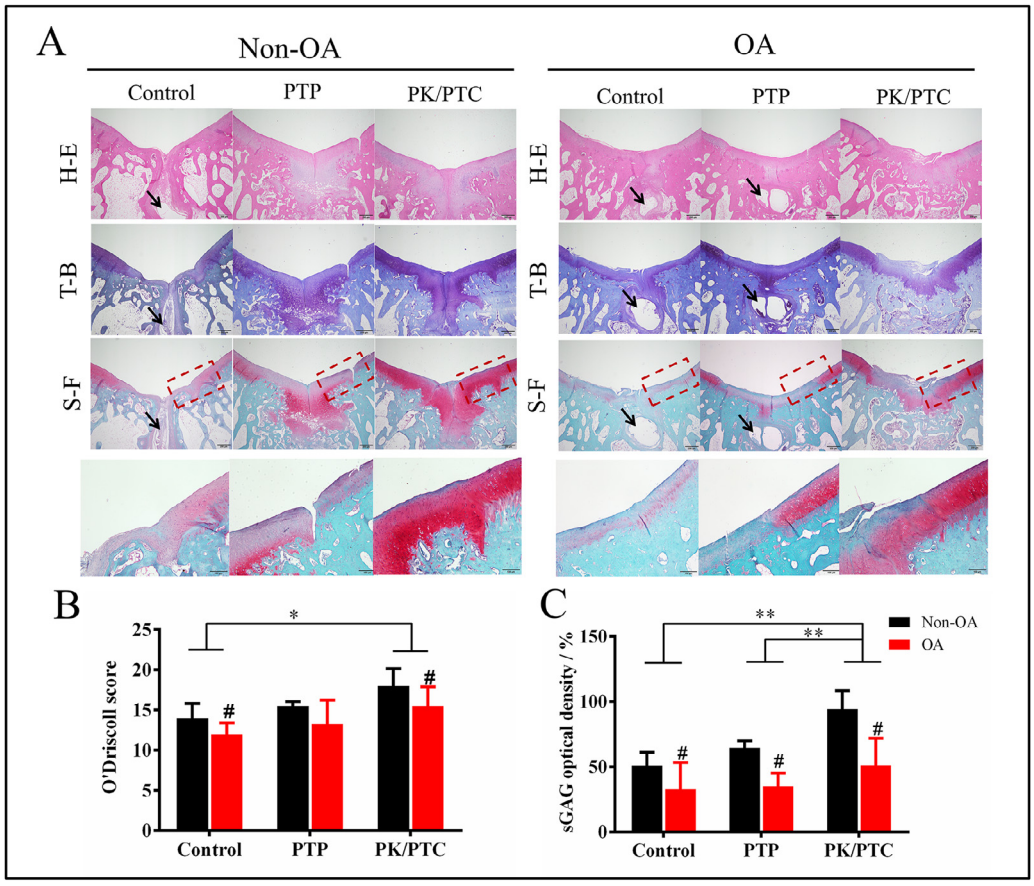

Fig. 4. Histological analysis of tissue repair at 16 weeks post-surgery. (A) Hematoxylin and eosin (H&E), toluidine blue (T-B), and Safranin O-fast green (S-F) showed enhanced cartilage repair in the PK/PTC group, compared to the PT group and the control group. The arrows denote the subchondral bone cyst. (B) The modified O'Driscoll histologic score (O'Driscoll) evaluation of OCD in rabbits. (C) Quantification of sulfated glycosaminoglycan (sGAG) optical density in new cartilage. Data are shown as mean ± standard deviation, $n = 4$, $^{\#}p < 0.05$ vs non-OA; $^{*}p < 0.05$ and $^{**}p < 0.01$. The black arrow indicates the subchondral cyst.

pore size of scaffolds play a critical role in bone formation [26,38]. Based on early studies, the minimum requirement for pore size is considered to be ~100 μm due to cell size, migration requirements, and transport. However, pore sizes > 300 μm are recommended, due to enhanced new bone formation and the formation of capillaries [26]. In this study, PTP scaffolds or PK/PTC scaffolds had a pore size larger than 450 μm and a porosity higher than 65%, which can support cell proliferation, differentiation, and vascular growth [33,39].

Degradation is an important physical property of the scaffolds. The PLGA copolymer undergoes degradation in aqueous mediums both *in vitro* and *in vivo* through the cleavage of its backbone ester linkage. The complete degradation of PLGA forms water soluble and acidic degradation products, namely, lactic and glycolic acids, which are removed from the body by normal metabolic pathways [40]. This decrease in pH is mainly because of the formation of these aqueous oligomers. Since these degradation products are acidic and retained in the incubation medium, then any polymer degradation will result in a reduction in pH.

At the early stage, the pH maintained around 7.0 for 37 days perhaps because of the limited formation of water-soluble oligomers. Similarly, in a previous study, it was found that the pH change was small, while the concentrations of both the lactic and glycolic acids were low during the early time of incubation time [41]. The pH value got lower as more lactic and glycolic acids formed with degradation. It declined when reaching the peak and finally raised to about 6.41. It also can be seen from Fig. S1 that the macro-structure of the scaffolds has disappeared morphology, and PK degraded into powder in the solution with pH = 6.56 at day 236.

Besides the pH value change to show the complete degradation of PLGA, calcium ions (Ca^{2+}) concentration in the degradation medium is an important indicator to monitor the degradation of TCP. In our recently published work [27], we measured the Ca^{2+} concentrations in the degradation medium at each time point to monitor the TCP degradation. In these two independent degradation experiments, pH value curves demonstrate a similar pattern, so we speculated that Ca^{2+} release had a similar pattern. It is well known that the PLGA copolymer undergoes the cleavage of its backbone ester linkage in aqueous mediums before complete degradation [40]. So, the average molecule weight of the left scaffold at each time point is important to monitor the degradation of PLGA. However, this will consume a lot of scaffolds, which hinder us from monitoring the degradation of PLGA in this study. Therefore, only recording the pH change in this process was the limitation of this study.

In vivo, the scaffolds were degraded and replaced by new tissues during the healing process after scaffold implantation [42]. At the same time, the scaffolds provided the necessary mechanical support and enough space for the growth of new tissue [43]. In this study, the PTP scaffold or the PK/PTC scaffold had sufficient mechanical strength to support bone tissue regeneration, which allows the adhesion of chondrocytes and osteoblasts. However, a limitation of this study is that no *in vivo* degradation of scaffolds was tested. The interaction between scaffold degradation and new tissue in-growth and maturation is difficult to be accurately de-

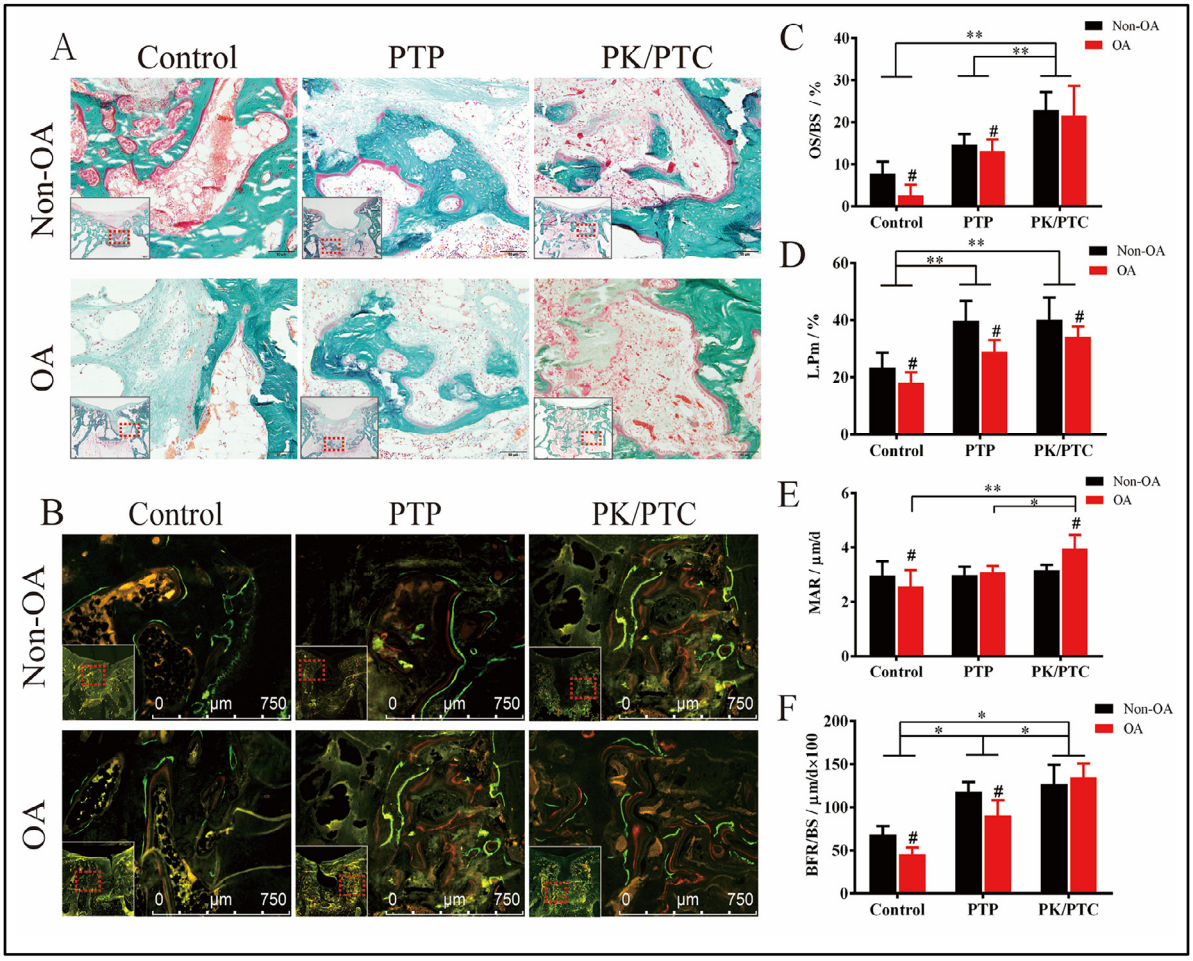

Fig. 5. Dynamic histomorphology evaluation of subchondral bone. (A) Goldner staining showed osteoid and osteoblasts in the defect site (Red: osteoid. Green: mineralized bone tissue); (B) New bone in the defect site labeled with calcein (green) and xylenol orange (red); (C) Osteoid surface/bone surface (OS/BS, %), (D) Percent labeled perimeter (L.Pm, %), (E) Mineral apposition rate (MAR, μm/day), and (F) Bone formation rate/bone surface (BFR/BS) were quantified respectively. Data are shown as mean ± standard deviation, $n = 4$, $^{\#}p < 0.05$ vs non-OA; $^{*}p < 0.05$ and $^{**}p < 0.01$.

scribed in animal experiments. In the present study, the scaffolds were implanted at a non-weight-bearing site (femoral trochlea), so the changed mechanical properties of the scaffolds during *in vivo* degradation had little effect on new bone regeneration. However, the degradation property of scaffold *in vivo* and the interaction between degradation scaffold and newly formed tissue should be investigated in the future.

4.2. PK/PTC scaffolds promote the synthesis of sGAG and COL II in the regenerated cartilage in vivo

KGN has been regarded as a promising small molecule to induce chondrogenesis of human bone mesenchymal stem cells (hBMSCs) by forming cartilage nodules *in vitro* [20]. Moreover, KGN ameliorated cartilage degradation and attenuated osteoarthritis progression *in vivo* [44]. The cartilage layer of biphasic scaffolds, incorporating KGN, can mimic the regenerative microenvironment, thereby promoting the differentiation of BMSCs into chondrocytes and the synthesis of the extracellular matrix of cartilage [30,45]. The PLGA enables sustained and localized delivery of bioactive molecules. In this study, the cumulative release of KGN from PK scaffold reached approximately 84.59% *in vitro*. Furthermore, *in vivo* evidence indicated that the cartilage defect was repaired at 16 weeks after implantation of PK/PTC scaffold. Notably, the regenerated cartilage binds to its surrounding tissue and subchondral bone. Histological examination showed that the PK/PTC group had more neocartilage than the control group and PTP group. Further, sGAG and COL II of neocartilage in the PK/PTC group were more abundant, compared with the control and PTP group, thereby improving the quantity and quality of regenerated tissue at the chondral interface.

4.3. PK/PTC scaffolds enhance osteogenesis and subchondral bone regeneration in OA joints

Our study found that intra-articular injection of papain in rabbits not only reduced the glycosaminoglycans content in articular cartilage but also significantly increased the BMD of subchondral bone in the femoral trochlea. However, in clinical or surgical OA models, the subchondral bone of the tibial plateau was usually considered. Because the subchondral bone changes in the tibial plateau were more obvious than that in the femur due to the mechanical factors [46]. In our study, the defect was created in the femoral trochlea, which provides us a possibility to investigate the mechanism of subchondral bone changes in OA without mechanical effects.

The mineral BMD of the new bone in the defect area and the host bone adjacent to the defect in the OA group increased significantly. Papain is a proteolytic enzyme that causes OA by releasing chondroitin sulfate from a protein-polysaccharide complex of the articular cartilage matrix and producing inflammatory cytokines, such as tumor necrosis factor-α (TNF-α) [47]. TNF-α in-

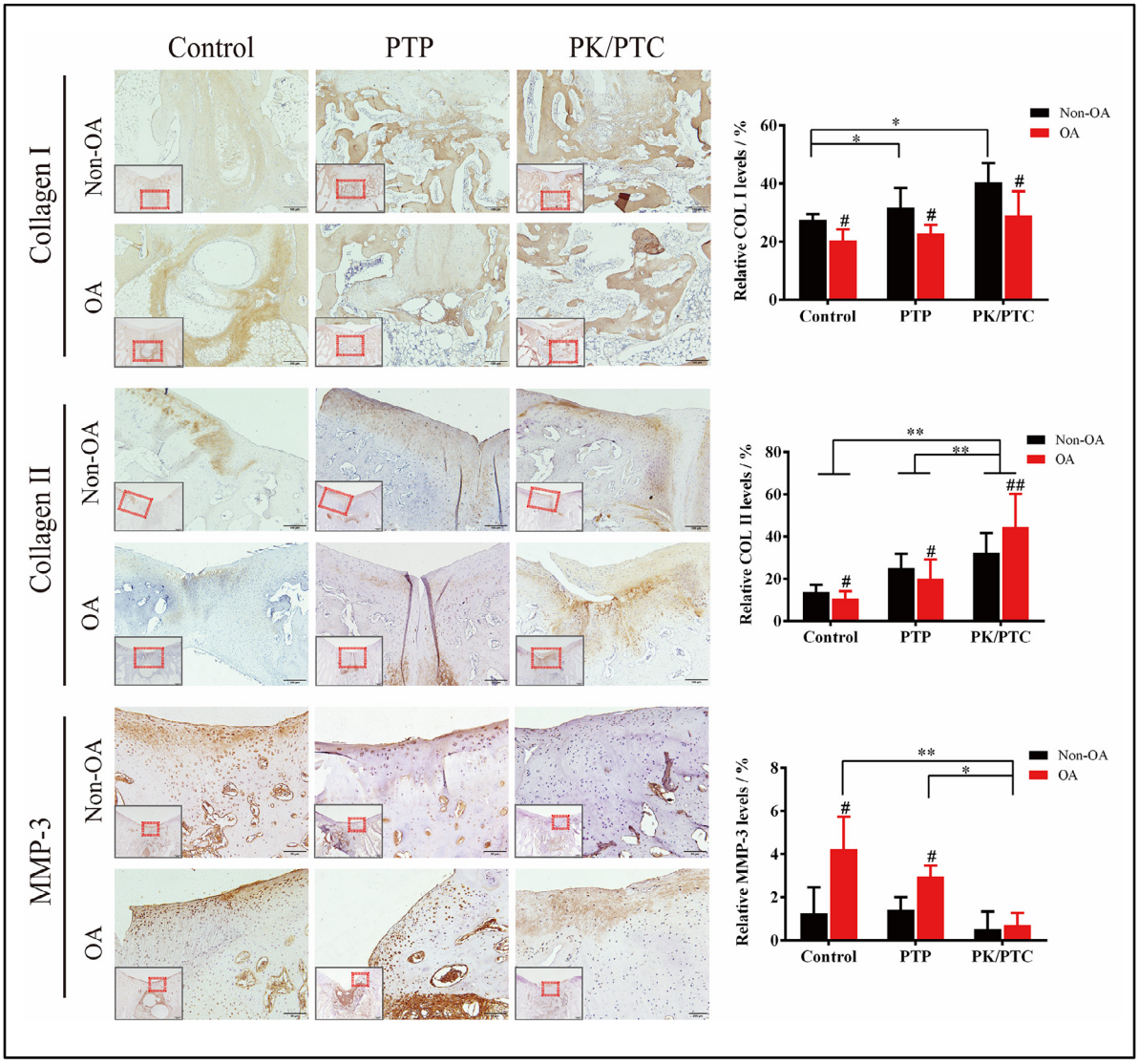

Fig. 6. Immunohistochemical staining for cartilage and bone-specific proteins. The collagen type I (COL I), collagen type II (COL II), and MMP-3 in sections were visualized at week 16. The quantitative results showed that both COL I and COL II were abundant in the new tissue of the PK/PTC group at week 16. The expression of MMP-3 in the new cartilage of the PK/PTC group was lower than that of the PTP and control groups. Data are shown as mean ± standard deviation, $n = 4$, $^{\#}p < 0.05$ vs non-OA; $^{*}p < 0.05$ and $^{**}p < 0.01$.

hibited osteoblastic proliferation and matrix synthesis and activating TNF receptor-associated Factor-2 (TRAF-2), which activated NF-κB, AP-1, and MAPKs signaling pathways and led to decreased bone formation [48]. However, in a human study, it was found that TNF-α inhibited Runx2 and collagen expression but increased alkaline phosphatase activity and matrix mineralization [49]. Therefore, TNF-α in the articular micro-environment may play important roles in increasing the mineral BMD of subchondral bone in this papain-induced rabbit model. It was also well known that TNF-α is a stimulator of osteoclastogenesis [50]. The osteoclastogenesis and bone resorption in this model should be investigated in the future study.

The osseous layer of biphasic scaffolds consists of PLGA, β-TCP, and CIN. Cinnamaldehyde, an essential active constituent of *Cinnamomum cassia*, could inhibit osteoclastogenesis and promote osteoblastogenesis [23]. In addition, CIN plus β-TCP enhanced bone formation [51]. The present study showed that the PTC scaffold showed better osteogenic potential compared with the PT scaffold, which indicated that the bioactivity of the CIN molecules released from the scaffold was retained. The CIN release curve showed that its cumulative release reached approximately 85.92% *in vitro*. *In vivo* histological images showed that the defects of the PK/PTC group were filled with new bone without a cyst. In addition, the IHC staining showed that COL I of the PK/PTC scaffold was positively expressed in regenerated tissues.

4.4. PK/PTC scaffolds attenuate cartilage degeneration in OA

The degeneration of cartilage is associated with primary clinical symptoms in the OA joint. Inflammation is a foremost factor in OA pathogenesis because it exacerbates pain and joint destruction [52]. Dysregulation between anabolic and catabolic factors is associated with cartilage destruction in the pathogenesis of OA [53]. It has been shown that matrix metalloproteinases (MMPs) accelerate cartilage degeneration and increase OA development [54]. Chen et al. [55] reported that the expression of MMP-3 protein was positively correlated with the severity of OA. In this study, papain destroyed articular cartilage and increased the expression of MMP-3. Compared with the PTP group, the expression of MMP-3 in the PK/PTC group was reduced, which might contribute to cartilage

degradation. Both KGN and CIN in the PK/PTC scaffold might play a role in anti-inflammation. Previous studies demonstrated that KGN inhibited chondrocyte inflammation, thereby reducing the progression of osteoarthritis [56,57]. In addition, our previous study found that CIN was able to inhibit inflammation *in vitro* and in collagen-induced arthritic rats [25].

This study also has some limitations. We used two molecules, KGN and CIN, to meet the requirements of anti-inflammation, bone regeneration, and cartilage regeneration. It is difficult to identify the roles of the individual molecule. The final effects are the result of the combined efficacy of the two bioactive factors. The interaction between them remains unknown. Also, the dose of each drug in the scaffold remains to be optimized in the future.

5. Conclusions

Based on the unique pathology of OA-OCD an innovative biphasic porous scaffold with bioactive molecules has been successfully fabricated, which demonstrates suitable pore size, high porosity, appropriate mechanical structure, and microenvironment to induce osteochondral regeneration. Anti-inflammatory and anabolic bioactive molecules KGN and CIN sustainably released from the biphasic porous scaffold can induce the regeneration of cartilage and subchondral bone, and reverse subchondral osteosclerosis in an OA-OCD rabbit model. The biphasic porous functional scaffold offers novel and effective approaches for repairing OA-OCD. Further translational studies will be performed to achieve clinical application in the future.

Declaration of Competing Interest

The authors declare that they have no known competing financial interests or personal relationships that could have appeared to influence the work reported in this paper.

CRediT authorship contribution statement

Xiangbo Meng: Investigation, Writing – review & editing. **Ling Li:** Formal analysis, Data curation. **Cuishan Huang:** Formal analysis, Data curation. **Keda Shi:** Data curation. **Qingqiang Zeng:** Data curation. **Chunyi Wen:** Conceptualization, Investigation. **Sibylle Grad:** Conceptualization, Investigation. **Mauro Alini:** Conceptualization, Investigation. **Ling Qin:** Conceptualization, Investigation. **Xinluan Wang:** Conceptualization, Investigation.

Acknowledgements

This work was supported by the collaborative project from the National Key R&D Program of China and Innovation and Technology Fund Mainland-Hong Kong Joint Funding Scheme (Nos. 2021YFE0202300 and MHP/011/20), the Sino-Swiss collaborative project from the Ministry of Science and Technology and the Swiss National Science Foundation under the SSSTC program (Grant Nos. 2015DFG32200 and 156362), Shenzhen Collaborative Innovation Plan-International Cooperation Project (Grant No. GJHZ20190821160803823), Development and Reform Commission of Shenzhen Municipality (2019) (No. 561) and Shenzhen Double Chain Project for Innovation and Development Industry supported by Bureau of Industry and Information Technology of Shenzhen (No. 201908141541).

Supplementary materials

Supplementary material associated with this article can be found, in the online version, at doi:10.1016/j.jmst.2023.01.035.

References

[1] S.G. Jones, A.J.R. Palmer, R. Agricola, A.J. Price, T.L. Vincent, H. Weinans, A.J. Carr, Osteoarthritis 386 (2015) 376–387.
[2] J.M. Oliveira, S. Pina, R.L. Reis, J.S. Roman, Osteochondral tissue Engineering: Challenges, Current Strategies and Technological Advances, Springer International Publishing AG, Cham, Switzerland, 2018.
[3] T. Gorbachova, Y. Melenevsky, M. Cohen, B.W. Cerniglia, Radiographics 38 (2018) 1478–1495.
[4] M. Tamaddon, L. Wang, Z.Y. Liu, C.Z. Liu, Bio-Des. Manuf. 1 (2018) 101–114.
[5] D.L. Richter, R.C. Schenck Jr, D.C. Wascher, G. Treme, Sports Health 8 (2016) 153–160.
[6] A.H. Gomoll, H. Madry, G. Knutsen, N.V. Dijk, R. Seil, M. Brittberg, E. Kon, Knee Surg. Sports Traumatol. Arthrosc. 18 (2010) 434–447.
[7] P. Angele, P. Niemeyer, M. Steinwachs, G. Filardo, A.H. Gomoll, E. Kon, J. Zellner, H. Madry, Knee Surg. Sports Traumatol. Arthrosc. 24 (2016) 1743–1752.
[8] X.L. Nie, Y.J. Chuah, W.Z. Zhu, P.F. He, Y. Peck, D.A. Wang, Biomaterials 235 (2020) 119821.
[9] C.C. Ai, Y.H.D. Lee, X.H. Tan, S.H.S. Tan, J.H.P. Hui, J.C. Goh, J. Orthop. Transl. 30 (2021) 93–102.
[10] S.E. Eldridge, A. Barawi, H. Wang, A.J. Roelofs, M. Kaneva, Z. Guan, H. Lydon, B.L. Thomas, A.S. Thorup, B.F. Fernandez, S. Caxaria, D. Strachan, A. Ali, K. Shanmuganathan, C. Pitzalis, J.R. Whiteford, F. Henson, A.W. McCaskie, C.D. Bari, F. Dell'Accio, Sci. Transl. Med. 12 (2020) eaax9086.
[11] T. Yang, M. Tamaddon, L. Jiang, J. Wang, Z.Y. Liu, Z.Q. Liu, H.Y. Meng, Y.Q. Hu, J.M. Gao, X. Yang, Y.X. Zhao, Y.L. Wang, A.Y. Wang, Q. Wu, C.Z. Liu, J. Peng, X.D. Sun, Q.Y. Xue, J. Orthop. Transl. 30 (2021) 112–121.
[12] D. Kilian, S. Cometta, A. Bernhardt, R. Taymour, J. Golde, T. Ahlfeld, J. Emmermacher, M. Gelinsky, A. Lode, Biofabrication 14 (2022) 014108.
[13] M.L. Bedell, A.M. Navara, Y.Y. Du, S.M. Zhang, A.G. Mikos, Chem. Rev. 120 (2020) 10744–10792.
[14] E.J. Lee, F.K. Kasper, A.G. Mikos, Ann. Biomed. Eng. 42 (2014) 323–337.
[15] G.S. Shi, Y.Y. Li, Y.P. Luo, J.F. Jin, Y.X. Sun, L.Z. Zheng, Y.X. Lai, L. Li, G.H. Fu, L. Qin, S.H. Chen, J. Orthop. Transl. 24 (2020) 112–120.
[16] D. Bicho, S. Ajami, C. Liu, R.L. Reis, J.M. Oliveira, J. Mater. Chem. B 7 (2019) 1027–1044.
[17] Y.X. Lai, H.J. Cao, X.L. Wang, S.K. Chen, M. Zhang, N. Wang, Z.H. Yao, Y. Dai, X.H. Xie, P. Zhang, X.S. Yao, L. Qin, Biomaterials 153 (2018) 1–13.
[18] S. Jin, X. Xia, J.H. Huang, C. Yuan, Y. Zuo, Y.B. Li, J.D. Li, Acta Biomater. 127 (2021) 56–79.
[19] Y.X. Lai, Y. Li, H.J. Cao, J. Long, X.L. Wang, L. Li, C.R. Li, Q.Y. Jia, B. Teng, T.T. Tang, J. Peng, D. Eglin, M. Alini, D.W. Grijpma, G. Richards, L. Qin, Biomaterials 197 (2019) 207–219.
[20] K. Johnson, S.T. Zhu, M.S. Tremblay, J.N. Payette, J.N. Wang, L.C. Bouchez, S. Meeusen, A. Althage, C.Y. Cho, X. Wu, P.G. Schultz, Science 336 (2012) 717–721.
[21] D.Q. Shi, X.Q. Xu, Y.Q. Ye, K. Song, Y.X. Cheng, J. Di, Q.Y. Hu, J.X. Li, H.X. Ju, Q. Jiang, Z. Gu, ACS Nano 10 (2016) 1292–1299.
[22] X. Yuan, L. Han, P. Fu, H.W. Zeng, C. Lv, W.L. Chang, R.S. Runyon, M. Ishii, L.W. Han, K.C. Liu, T.P. Fan, W.D. Zhang, R.H. Liu, Lab. Invest. 98 (2018) 783–798.
[23] Z.Y. Wu, S.J. Weng, D.Y. Yan, Z.J. Xie, Q. Zhou, H. Li, B.L. Bai, V. Boodhun, Z.J. Shen, J.H. Tang, L.L. Zhou, Z.S. Tao, L. Yang, J. Pharmacol. Sci. 138 (2018) 63–70.
[24] W.X. Cheng, S. Zhong, X.B. Meng, N.Y. Zheng, P. Zhang, Y. Wang, L. Qin, X.L. Wang, J. Pharmacol. Exp. Ther. 373 (2020) 302–310.
[25] X.B. Meng, S. Grad, C.Y. Wen, Y.X. Lai, M. Alini, L. Qin, X.L. Wang, J. Orthop. Transl. 26 (2021) 101–110.
[26] V. Karageorgiou, D. Kaplan, Biomaterials 26 (2005) 5474–5491.
[27] H.J. Cao, L.L. Li, L. Li, X.B. Meng, Y.Z. Liu, W.X. Cheng, P. Zhang, Y.B. Gao, L. Qin, X.L. Wang, J. Orthop. Transl. 36 (2022) 52–63.
[28] J.M. Xu, C.Q. Zhang, In Vitro Cell. Dev. Biol. Anim. 50 (2014) 623–629.
[29] S. Shen, H. Wang, J. Zhang, F. Wang, M. Chen, BMC Musculoskelet. Disord. 16 (2015) 361–371.
[30] Y.Z. Liu, L.Q. Peng, L.L. Li, C.S. Huang, K.D. Shi, X.B. Meng, P.P. Wang, M.M. Wu, L. Li, H.J. Cao, K.F. Wu, Q.Q. Zeng, H.B. Pan, W.W. Lu, L. Qin, C.S. Ruan, X.L. Wang, Biomaterials 279 (2021) 121216.
[31] Y.Y. Du, H.M. Liu, Q. Yang, S. Wang, J.L. Wang, J. Ma, I. Noh, A.G. Mikos, S.M. Zhang, Biomaterials 137 (2017) 37–48.
[32] L. Bi, D. Li, J. Liu, Y.Y. Hu, P. Yang, B. Yang, Z. Yuan, Mater. Lett. 65 (2011) 2079–2082.
[33] X. Pei, L. Ma, B.Q. Zhang, J.X. Sun, Y. Sun, Y.J. Fan, Z.R. Gou, C.C. Zhou, X.D. Zhang, Biofabrication 9 (2017) 045008.
[34] Y.H. Chen, S.W. Zhou, Q. Li, Biomaterials 32 (2011) 5003–5014.
[35] S. Am, N. Mohamed, I.N. Soelaiman, Med. Health. 11 (2016) 278–288.
[36] W.X. Cheng, Y.Z. Liu, X.B. Meng, Z.T. Zheng, L.L. Li, L.Q. Ke, L. Li, C.S. Huang, G.Y. Zhu, H.D. Pan, L. Qin, X.L. Wang, P. Zhang, J. Orthop. Transl. 31 (2021) 41–51.
[37] X.L. Wang, X.H. Xie, G. Zhang, S.H. Chen, D. Yao, K. He, X.H. Wang, X.S. Yao, Y. Leng, K.P. Fung, K.S. Leung, L. Qin, J. Orthop. Res. 31 (2013) 164–172.
[38] C. Torres-Sanchez, F.R.A. Al Mushref, M. Norrito, K. Yendall, Y. Liu, P.P. Conway, Mater. Sci. Eng. C-Mater. Biol. Appl. 77 (2017) 219–228.
[39] K. Rezwan, Q.Z. Chen, J.J. Blaker, A.R. Boccaccini, Biomaterials 27 (2006) 3413–3431.
[40] L. Lu, S.J. Peter, M.D. Lyman, H.L. Lai, S.M. Leite, J.A. Tamada, S. Uyama, J.P. Vacanti, R. Langer, A.G. Mikos, Biomaterials 21 (2000) 1837–1845.

[41] A.S. Hussein, N. Abdullah, F.R. Ahmadun, IET Nanobiotechnol. 7 (2013) 33–41.
[42] D.Y. Zhao, T.T. Zhu, J. Li, L.G. Cui, Z.Y. Zhang, X.L. Zhuang, J.X. Ding, Bioact. Mater. 6 (2021) 346–360.
[43] K.M. Kennedy, A. Bhaw-Luximon, D. Jhurry, Acta Biomater. 50 (2017) 41–55.
[44] M.Z. Hou, Y.J. Zhang, X.F. Zhou, T. Liu, H.L. Yang, X. Chen, F. He, X.S. Zhu, Cell Death Dis. 12 (2021) 483–499.
[45] Y.H. Zhao, X.G. Zhao, R. Zhang, Y. Huang, Y.J. Li, M.H. Shan, X.T. Zhong, Y. Xing, M. Wang, Y. Zhang, Y.M. Zhao, Front. Bioeng. Biotechnol. 8 (2020) 600103.
[46] K. Chiba, M. Uetani, Y. Kido, M. Ito, N. Okazaki, K. Taguchi, H. Shindo, Osteoporos Int. 23 (2012) 589–597.
[47] K. Lampropoulou-Adamidou, P. Lelovas, E.V. Karadimas, C. Liakou, I.K. Triantafillopoulos, I. Dontas, N.A. Papaioannou, Eur. J. Orthop. Surg. Traumatol. 24 (2014) 263–271.
[48] L. Gilbert, X.F. He, P. Farmer, S. Boden, M. Kozlowski, J. Rubin, M.S. Nanes, Endocrinology 141 (2000) 3956–3964.
[49] J. Ding, O. Ghali, P. Lencel, O. Broux, C. Chauveau, J.C. Devedjian, P. Hardouin, D. Magne, Life Sci. 84 (2009) 499–504.
[50] B. Osta, G. Benedetti, P. Miossec, Front. Immunol. 5 (2014) 48–57.
[51] S.J. Weng, D.Y. Yan, J.H. Tang, Z.J. Shen, Z.Y. Wu, Z.J. Xie, J.Y. Yang, B.L. Bai, L. Chen, V. Boodhun, L. Yang, X.D.E. Dong, L. Yang, Biomed. Pharmacother. 109 (2019) 573–581.
[52] P. Wojdasiewicz, L.A. Poniatowski, D. Szukiewicz, Mediat. Inflamm. 2014 (2014) 561459.
[53] A. Mobasheri, M.P. Rayman, O. Gualillo, J. Sellam, P.V.D. Kraan, U. Fearon, Nat. Rev. Rheumatol. 13 (2017) 302–311.
[54] E.E. Mehana, A.F. Khafaga, S.S. El-Blehi, Life Sci. 234 (2019) 116786.
[55] J.J. Chen, J.F. Huang, W.X. Du, P.J. Tong, Asian Pac, J. Trop. Med. 7 (2014) 297–300.
[56] J.Y. Kwon, S.H. Lee, H.S. Na, K. Jung, J. Choi, K.H. Cho, C.Y. Lee, S.J. Kim, S.H. Park, D.Y. Shin, M.L. Cho, Sci. Rep. 8 (2018) 13832.
[57] S.J. Wang, J.Z. Qin, T.E. Zhang, C. Xia, Front. Chem. 7 (2019) 677–685.